

A shared law between sources of repeating fast radio bursts

Mohammed A. Chamma,^{1*} Fereshteh Rajabi,^{2,3} Christopher M. Wyenberg,¹
Abhilash Mathews,⁴, Martin Houde,^{1†}

¹Department of Physics and Astronomy, The University of Western Ontario,
1151 Richmond Street, London, Ontario N6A 3K7, Canada

²Institute for Quantum Computing and Department of Physics and Astronomy,
The University of Waterloo, 200 University Ave. West,
Waterloo, Ontario N2L 3G1, Canada

³Perimeter Institute for Theoretical Physics,
Waterloo, ON N2L 2Y5, Canada

⁴Plasma Science and Fusion Center, Massachusetts Institute of Technology,
77 Massachusetts Avenue, Cambridge, MA 02139, USA

*Mohammed A. Chamma; E-mail: mchamma@uwo.ca.

†Martin Houde; E-mail: mhoude2@uwo.ca.

We study the spectro-temporal characteristics of two repeating fast radio bursts (FRBs), namely, FRB 180916.J0158+65 and FRB 180814.J0422+73, and combine the results with those from our earlier analysis on FRB 121102. The relationship between the frequency drift rate of individual sub-bursts and their temporal duration is investigated. We verify the existence of the inverse scaling law between the two parameters previously predicted using a simple dynamical relativistic model for all sources. The remarkably similar behavior observed in all sources provides strong evidence that a single and common un-

derlying physical phenomenon is responsible for the emission of signals from these three FRBs, despite their associations with different types of host galaxies at various redshifts. It also opens up the possibility that this sub-burst drift law may be a universal property among repeating FRBs, or at least for a significant subclass among them.

Introduction

Fast radio bursts are short duration (\sim millisecond) bursts of energy at radio wavelengths exhibiting large brightness temperatures ($T_B > 10^{32}$ K) (1, 2), indicating that these signals originate from non-thermal objects through some coherent emission mechanism. Still, the origin and underlying physical mechanism of FRBs remain unknown in spite of the large number of proposed models. FRB signals also undergo a high level of dispersion as they propagate from the source to the observer, a phenomenon quantified through the dispersion measure (DM). This dispersion results from the wavelength dependence of the refractive index of ionized matter in astronomical media through which radiation travels at varying speeds as a function of frequency. While a first Galactic FRB was recently reported by the CHIME/FRB Collaboration toward the Galactic magnetar SGR 1935+2154 (3), the DM values measured for most FRBs suggest that these signals must emanate from extragalactic sources.

Reported FRBs fall into two groups: one-off events and repeaters. While one-off events form the majority of detections, most of our knowledge about FRBs is based on the study of repeaters. At the time of writing, two repeaters (FRB 121102 and FRB 180916.J0158+65) show periodic behaviours, prompting continued follow-up observations (4, 5). Importantly, the study of dynamic spectra of repeaters reveals interesting patterns. Among these are a downward drift in the central frequency of consecutive sub-bursts with increasing arrival time within an event (the so-called “sad trombone” effect), and a reduction in the temporal duration of individual

sub-bursts with increasing frequency (6–9).

Several models have been proposed to explain these spectro-temporal characteristics. Some models link these characteristics to the intrinsic radiation mechanism of FRBs (10–12) or propagation effects (e.g., plasma lensing (13) or scintillation (14)), while others argue that a combination of both factors can play a part (7). Recently, the detection of the first Galactic FRB (3, 15) has posed new challenges for existing theoretical models. For example, one sequence of sub-bursts detected toward this source reveals an upward central frequency drift with increasing arrival time (a “happy trombone” effect). A few models have anticipated such a possibility for the spectra of FRBs (14, 16, 17). In particular, in Rajabi et al. (2020) (16) we proposed a simple dynamical relativistic model where a descending or an ascending central frequency drift for a sequence of sub-bursts can be explained based on the intrinsic properties of the corresponding FRB source. But more importantly, our model also predicts that a steeper frequency drift should be present within individual sub-bursts (henceforth the sub-burst drift) where the slope of the FRB signal as displayed in a dynamical spectrum (i.e., frequency vs. time) obeys a simple law scaling inversely with the temporal duration of the sub-burst. We further provided evidence for this sub-burst drift behavior for FRB 121102 and showed that data taken over a wide range of frequencies for this repeater follows the same law, i.e., the aforementioned inverse scaling of the sub-bursts drift with their corresponding temporal duration. We then argued that this finding implies that the underlying physical process responsible for the signals detected in FRB 121102 is intrinsically narrow-band in nature, while relativistic motions within the source are required to explain the wide observed bandwidths. In this paper, we examine data from two additional repeaters, FRB 180814.J0422+73 (8) and FRB 180916.J0158+65 (18), and show that this same law is shared among these three FRBs originating from host galaxies at different redshifts. This significant finding reveals new insights on the underlying physical mechanism at the source of FRB signals and helps refine modelling efforts.

Results and Discussion

In Rajabi et al. (2020) (16) we introduced a simple dynamical model where a triggering source (e.g., a pulsar or magnetar; see (19)) is located directly behind an FRB source, as seen by an observer. The regions from which FRB signals are emanating are assumed to be moving towards (or away from) the observer, potentially at relativistic speeds. Such a scenario is appropriate for situations where the emitted signal is highly collimated, such as is the case for a radiation process based on Dicke’s superradiance on which our proposed FRB model is ultimately built upon (20–26). Under such conditions we showed that the sub-burst drift from a single FRB signal (for repeaters an event can contain several sub-bursts) obeys the following relation

$$\frac{1}{\nu_{\text{obs}}} \frac{d\nu_{\text{obs}}}{dt_D} = -\frac{A}{t_w}, \quad (1)$$

where ν_{obs} , t_w and t_D are the frequency, the temporal duration of the FRB sub-burst and the delay before its appearance (in relation to the arrival of the trigger) as measured by the observer. The systemic parameter $A \equiv \tau'_w / \tau'_D$ with τ'_w and τ'_D the corresponding sub-burst proper temporal duration and delay in the FRB reference frame, respectively.

Although equation (1) was tested and verified for FRB 121102 in (16) using previously published data covering more than a decade in frequency (6, 9, 27), it was not known at the time whether it applies equally well to other repeating FRBs. We therefore retrieved and analyzed previously published data for two other sources discovered by the CHIME/FRB Collaboration (28), namely FRB 180916.J0158+65 (18) and FRB 180814.J0422+73 (8). These data are all contained within the CHIME/FRB spectral band (approximately 400–800 MHz) and the corresponding dynamic spectra were analyzed using the two-dimensional autocorrelation technique introduced in (7), resulting in estimates for the sub-burst drift ($d\nu_{\text{obs}}/dt_D$) and temporal duration (t_w); see the SM section for more details.

We show in Figure 1 the results of our analysis, where the sub-burst drift rate (normal-

ized to the frequency of observation ν_{obs}) is plotted against the temporal width t_w for the three FRBs. Normalizing the sub-burst drift has the advantage of allowing us to combine the different sources on the same graph irrespective of the frequency of observation, shifts due to the dynamical Doppler effect or cosmological redshift. Furthermore, we note that equation (1) is also insensitive to temporal scaling transformations. For example, interstellar scintillation, which brings a temporal broadening scaling inversely with the fourth power of the frequency, will have no effect on our analysis. The only consequence being a shift of data points along the specific law characterized by the parameter A in equation (1). Examination of Figure 1 reveals that the inverse relationship between the two parameters is clearly seen for all sources on the graph for values ranging over two orders of magnitude for both the normalized sub-burst drift rate and the temporal duration. Also shown in the figure are fits for the predicted function A/t_w (see equation (1)) for the three sources independently, with $A = 0.082 \pm 0.006$, 0.082 ± 0.006 and 0.071 ± 0.010 for FRB 121102, FRB 180916.J0158+65 and FRB 180814.J0422+73, respectively.

A few important consequences are to be noted from the results presented in Figure 1. First, not only is the inverse relationship between the sub-burst drift and duration verified for the three sources, but they do so with similar values for A in equation (1). The different fits to this systemic parameter are similar given their uncertainties, and it is difficult to visually distinguish between the corresponding curves. This closeness between the values obtained for A is rather remarkable and points to the existence of a single and common underlying physical phenomenon responsible for the emission of FRB signals in the three sources. This is significant because these FRBs are associated with different types of host galaxies at various redshifts. More precisely, FRB 121102 is localized to a low-metallicity irregular dwarf galaxy at a redshift $z = 0.193$ (29), while the redshift of FRB 180814.J0422+73 is estimated to be $z \leq 0.1$ (8). Fur-

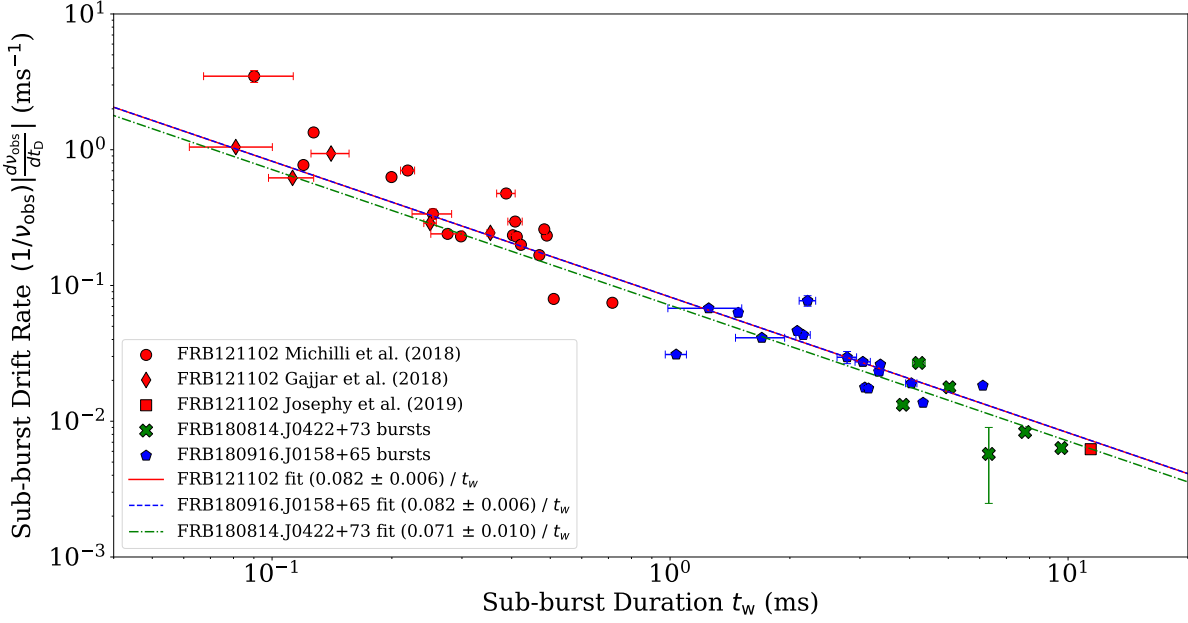


Figure 1: A plot of $(1/\nu_{\text{obs}}) |d\nu_{\text{obs}}/dt_{\text{D}}|$ vs. t_w for FRB 121102 (red circles, diamonds and square) (6, 9, 27), FRB 180916.J0158+65 (blue pentagons) (18) and FRB 180814.J0422+73 (green crosses) (8). The sub-burst drift $d\nu_{\text{obs}}/dt_{\text{D}}$ and duration t_w were obtained using the two-dimensional autocorrelation technique of Hessels et al. (2019) (7), while the center frequency ν_{obs} was estimated from the corresponding dynamic spectra. The red, blue and green lines are for fits of the function A/t_w on the FRB 121102, FRB 180916.J0158+65 and FRB 180814.J0422+73 data, respectively, and are difficult to distinguish from one another. See the supplementary text for the DM used for each source. Error bars shown only account for uncertainties derived from the underlying Gaussian fit of the autocorrelation function and do not reflect uncertainties caused by, for example, de-dispersion of the data.

thermore, the candidates for the host galaxy of FRB 180814.J0422+73 are not consistent with those harboring long gamma-ray bursts (LGRBs) or superluminous supernovae (SLSNe), unlike the host galaxy of FRB 121102 (30). As for FRB 180916.J0158+65, it is precisely localized to a star-forming region in a massive spiral galaxy at a redshift $z = 0.0337$ (31). This source is the closest known extragalactic FRB, whose host galaxy does not show signatures of a strong magnetic field nor a radio counterpart as reported for FRB 121102.

Second, and as was discussed in (16), the three predictions made by our simple dynami-

cal model (i.e., the narrowing of sub-bursts width t_w with increasing frequency ν_{obs} , the sad or happy trombone effect and the sub-burst drift law discussed here) provide strong evidence that the underlying physical phenomenon is narrow-band in nature. This is because the dependencies on ν_{obs} and the frequency of emission in the FRB rest frames ν_0 for three predicted relationships are such that it would be difficult to envision how they could be realized through the data if ν_0 was allowed to vary substantially (see the SM for more details). Although data over a significant range of observed frequency is currently only available for FRB 121102 (and constitutes the basis of the analysis presented in (16)), the fact that FRB 180916.J0158+65 and FRB 180814.J0422+73 follow the same law renders it reasonable to expect that the conclusions reached for FRB 121102 also apply to them.

We can use this information with our model to further characterise the environment of the sources responsible for the detected bursts. Indeed using the extensive data available for FRB 121102 one can estimate, although with limited precision at this point, the maximum Lorentz factor and the rest frame frequency of emission ν_0 . To do so we will assume highly simplified conditions, i.e., that the different FRB reference frames from which the sub-bursts emanate either move towards or away from the observers with the same range of speeds. We will denote by $\beta^+ > 0$ and $\beta^- = -\beta^+$ the maximum velocities (divided by the speed of light) towards and away from the observer, respectively, with corresponding observed frequencies ν_{obs}^\pm . It is then straightforward to show that, under this assumption,

$$\beta^+ = \frac{\nu_{\text{obs}}^+ - \nu_{\text{obs}}^-}{\nu_{\text{obs}}^+ + \nu_{\text{obs}}^-} \quad (2)$$

$$\nu_0^2 = \nu_{\text{obs}}^+ \nu_{\text{obs}}^- . \quad (3)$$

Using $\nu_{\text{obs}}^+ \approx 7.5$ GHz and $\nu_{\text{obs}}^- \approx 630$ MHz we find $\beta^+ \approx 0.9$ and $\nu_0 \approx 2.6$ GHz for FRB 121102 (taking into account its known redshift $z = 0.193$ (29); see the SM for more details). Evidently, the accuracy for these estimates is set and limited by the frequency cover-

age of the existing data and is likely to change as more detections are acquired. For example, confirming the purported detection of signals at 111 MHz from (32) would further increase β^+ and bring down ν_0 on the order of 1 GHz. At any rate, these results imply that FRB 121102 is potentially very strongly relativistic.

We also know that the spectral width $\Delta\nu_{\text{obs}}$ associated to sub-bursts for FRB 121102 scales as $\Delta\nu_{\text{obs}} \sim 0.16 \nu_{\text{obs}}$ (see Figure 6 in (16) or Figure 5 in (19)). This spectral extent is the result of motions within a given FRB rest frame from where a sub-burst centred at ν_{obs} originates. As discussed in the SM section, the observed spectral width is constrained through

$$2\Delta\beta' \leq \frac{\Delta\nu_{\text{obs}}}{\nu_{\text{obs}}} \leq \frac{2\Delta\beta'}{1 - \Delta\beta'^2}, \quad (4)$$

where the motions in the FRB rest frame are contained within $\pm\Delta\beta'$. We thus find $\Delta\beta' \sim 0.08$ with equation (4) for this source.

We thus have a picture where FRB 121102 and similar sources would consist of systems within which a number of spatially distinct FRB rest frames, whose motions cover a wide range of velocities (some highly relativistic relative to the observer), are responsible for the emission of individual sub-bursts. In turn, each such rest frame is also host to mildly relativistic motions, which are responsible for the observed wide spectral widths of sub-bursts.

Finally, we note that our discovery of a shared sub-burst drift law among these three sources suggests that this could be a universal property among repeating FRBs or at least a significant subclass of them. This not only motivates further searches but also provides a new tool to study and categorize FRBs based on their underlying physical mechanism.

References and Notes

1. D. R. Lorimer, M. Bailes, M. A. McLaughlin, D. J. Narkevic, F. Crawford, *Science* **318**, 777 (2007).

2. E. Petroff, J. Hessels, D. Lorimer, *The Astronomy and Astrophysics Review* **27**, 4 (2019).
3. B. Andersen, *et al.*, *arXiv preprint arXiv:2005.10324* (2020).
4. M. Amiri, *et al.*, *Nature* **582**, 351 (2020).
5. K. Rajwade, *et al.*, *Mon. Not. R. Astron. Soc.* **495**, 3551 (2020).
6. V. Gajjar, *et al.*, *Astrophys. J.* **863**, 2 (2018).
7. J. W. T. Hessels, *et al.*, *Astrophys. J.* **876**, L23 (2019).
8. CHIME/FRB Collaboration, *et al.*, *Nature* **566**, 235 (2019).
9. A. Josephy, *et al.*, *Astrophys. J.* **882**, L18 (2019).
10. W. Wang, B. Zhang, X. Chen, R. Xu, *Astrophys. J.* **876**, L15 (2019).
11. A. M. Beloborodov, *Astrophys. J.* **896**, 142 (2020).
12. B. D. Metzger, B. Margalit, L. Sironi, *Mon. Not. R. Astron. Soc.* **485**, 4091 (2019).
13. J. M. Cordes, *et al.*, *Astrophys. J.* **842**, 35 (2017).
14. D. Simard, V. Ravi, *Astrophys. J.* **899**, L21 (2020).
15. P. Scholz, CHIME/FRB Collaboration, *The Astronomer's Telegram* **13681**, 1 (2020).
16. F. Rajabi, M. A. Chamma, C. M. Wyenberg, A. Mathews, M. Houde, *Mon. Not. R. Astron. Soc.* **498**, 4936 (2020).
17. P. Beniamini, P. Kumar, *Mon. Not. R. Astron. Soc.* **498**, 651 (2020).
18. P. Chawla, *et al.*, *Astrophys. J.* **896**, L41 (2020).

19. M. Houde, F. Rajabi, B. M. Gaensler, A. Mathews, V. Tranchant, *Mon. Not. R. Astron.* **482**, 5492 (2019).
20. F. Rajabi, M. Houde, *Astrophys. J.* **826**, 216 (2016).
21. F. Rajabi, M. Houde, *Astrophys. J.* **828**, 57 (2016).
22. F. Rajabi, M. Houde, *Science Advances* **3**, e1601858 (2017).
23. A. Mathews, The role of superradiance in cosmic fast radio bursts, Honours thesis, The University of Western Ontario (2017).
24. M. Houde, A. Mathews, F. Rajabi, *Mon. Not. R. Astron.* **475**, 514 (2018).
25. F. Rajabi, *et al.*, *Mon. Not. R. Astron.* **484**, 1590 (2019).
26. F. Rajabi, M. Houde, *Mon. Not. R. Astron.* **494**, 5194 (2020).
27. D. Michilli, *et al.*, *Nature* **553**, 182 (2018).
28. E. Fonseca, *et al.*, *Astrophys. J.* **891**, L6 (2020).
29. S. P. Tendulkar, *et al.*, *Astrophys. J.* **834**, L7 (2017).
30. Y. Li, B. Zhang, K. Nagamine, J. Shi, *Astrophys. J.* **884**, L26 (2019).
31. B. Marcote, *et al.*, *Nature* **577**, 190 (2020).
32. V. A. Fedorova, A. E. Rodin, *Astronomy Reports* **63**, 39 (2019).
33. J. D. Hunter, *Computing in Science & Engineering* **9**, 90 (2007).
34. W. H. Press, S. A. Teukolsky, W. T. Vetterling, B. P. Flannery, *Numerical Recipes 3rd Edition: The Art of Scientific Computing* (Cambridge University Press, USA, 2007), third edn.

35. G. B. Rybicki, A. P. Lightman, *Radiative processes in astrophysics* (New York: Wiley, 1979).

Acknowledgments: The authors are grateful to Z. Pleunis and S. Tendulkar from the CHIME-FRB Collaboration for their help in accessing and analyzing the data for FRB 180916.J0158+65 and FRB 180814.J0422+73. M.H. is grateful for the hospitality of Perimeter Institute where part of this work was carried out. **Funding:** M.H.’s research is funded through the Natural Sciences and Engineering Research Council of Canada Discovery Grant RGPIN-2016-04460. F.R.’s research at Perimeter Institute is supported in part by the Government of Canada through the Department of Innovation, Science and Economic Development Canada and by the Province of Ontario through the Ministry of Economic Development, Job Creation and Trade. F.R. is in part financially supported by the Institute for Quantum Computing. C.M.W. and A.M. are supported by the Natural Sciences and Engineering Research Council of Canada (NSERC) through the doctoral postgraduate scholarship (PGS D). **Authors contributions:** M.A.C. obtained most of the data, developed the tools to analyze, and analyzed, the data, produced all but one figure, the Material and Methods section of the SM and helped with the main body of the text. F.R. and M.H. led the writing of the main body of the paper, wrote part of the SM and oversaw the project. A.M. and C.M.W. helped writing the main body of the text, and C.M.W. wrote part of the SM. **Competing interests:** The authors declare that they have no competing interests. **Data and materials availability:** The data pipeline is made available at <https://github.com/mef51/sadtrombone> and maintained by M.A.C. Aggregate data of the bursts and the code for the figures are also available. Data of the FRB spectra are available either publicly or via the authors of their respective publications. The figures in this paper were prepared using the `matplotlib` package (33).

Supplementary materials

Materials and Methods

This section will describe the process of deriving measurements of the sub-burst drift rate and the burst duration from dynamic spectra of Fast Radio Bursts (FRBs), and is largely based on the autocorrelation technique described in (7, 9). In addition, we describe tests to the robustness of the inverse trend between the sub-burst drift rate and duration through variations of the dispersion measure (DM). This will show that small variations of the DM rotate the autocorrelation function calculated from dynamic spectra of FRBs, and, even though they affect the measured value of the sub-burst drift rate, do not affect the relative trend between sub-bursts.

Dynamic spectra of bursts are obtained from several sources and processed based on the format they are made available in, and are typically de-dispersed to the DMs presented in their respective publications. Bursts from the repeater FRB 121102 were obtained from (6, 9, 27). These data were taken as presented in Figure 2 of (6), Figure 1 of (27) and Figure 5 of (9), and range in frequency from about 600 MHz to 8 GHz. For all bursts used from FRB 121102, we adopted the structure-optimized de-dispersed spectra without modification, which corresponds to DMs of 565, 559.7, and 563.6 pc cm⁻³ from (6, 9, 27), respectively.

Data for FRB 180916.J0158+65 and FRB 180814.J0422+73 are available from the public archive for the CHIME telescope (chime-frb-open-data.github.io) (4, 8). De-dispersed bursts from FRB 180916.J0158+65 are used at the published DM of 348.82 pc cm⁻³, though we also investigated the effect of small variations from this DM, as discussed later. Data for FRB180814.J0422+74 are also provided on the CHIME/FRB archive at their original resolution and without de-dispersion. The range of DMs used for this source in (8) vary between 188.9–190 pc cm⁻³. We find a good fit between these data and our model for DMs between 188.9–189.4 pc cm⁻³ but settled on a DM of 188.9 pc cm⁻³ for our analysis. We will argue that

the shape of the FRB 180814.J0422+7 sub-bursts suggests too aggressive of a de-dispersion for some of the higher DM values. In all cases, dynamic spectra are down-sampled in frequency as described in their original publications to increase the signal-to-noise ratio (SNR). When a dynamic spectrum consists of a train of multiple sub-bursts, whenever possible we separate the components and measure the drift rate and duration of each sub-burst separately, as described for Figure 3 of (16). Sub-bursts can be excluded from the analysis if the SNR is too low, or if the signal appears to be severely clipped at the top or bottom of the band or by noise masking. The dynamic spectra of every burst used in this analysis with its autocorrelation is shown in Figures 6 – 10 that will be found at the end.

Even when emanating from the same source, FRBs can have DMs that differ and also potentially vary with time (6), which raises questions about what DM is appropriate to use for our analysis. For this work (i.e., for FRB 180916.J0158+65 and FRB 180814.J0422+73) we choose a single DM per source since multiple sub-bursts from short duration pulse trains (which should be expected to have a single canonical DM) obey the inverse relationship between the sub-burst drift rate and duration discussed in the main text of our paper, and therefore supports the simplification of using a single DM for the analysis. We found that small variations in the DM (on the order of 1%) can increase the spread of the points and move them on the sub-burst drift vs. duration plot (i.e., Figure 1), which clearly affects the fit, but the existence of the relationship generally remains. Therefore, we limit ourselves to the range of DMs found from all the sub-bursts taken as a whole when considering variations, and for the analysis proper we select a single DM for all sub-bursts from a particular source. This will be discussed in more details shortly.

The general pipeline that every sub-burst is put through is written in Python and consists of computing the autocorrelation of the signal, fitting a two-dimensional (2D) Gaussian to the resulting autocorrelation function, and a calculation of the physical quantities of interest from

the fit parameters: namely the sub-burst drift rate and duration. The autocorrelation of the dynamic spectrum measures the self-similarity of the sub-burst in frequency-time space and for FRBs can be approximated by an ellipsoid with an intensity that follows a 2D Gaussian (7). Before computing the autocorrelation and depending on the source and/or burst, some noise removal is performed. For the bursts from FRB 121102 and FRB 180916.J0158+65 this is done by subtracting from the entire spectrum a background signal obtained from a time-average of twenty or so samples taken prior to the burst. For FRB 180814.J0422+73, due to the raw format the bursts are provided in, a noise mask was acquired through correspondence with members of the CHIME/FRB Collaboration and the channels are normalized by the standard deviation of the intensity. Missing or blocked out frequency channels in dynamic spectra (e.g., because of radio frequency interference (RFI)) are zeroed out before performing the autocorrelation (see below).

The computation of the autocorrelation function is facilitated and sped up by using a Fast Fourier Transform (FFT) of the dynamic spectrum, which is then squared and inverted (through an FFT) back to the frequency-time domain (34). The autocorrelation function is then modelled with the following functional form for a rotated 2D Gaussian

$$G(x, y) = C \exp \left\{ -\frac{1}{2} \left[x^2 \left(\frac{\cos^2 \theta}{b^2} + \frac{\sin^2 \theta}{a^2} \right) + 2xy \sin \theta \cos \theta \left(\frac{1}{b^2} - \frac{1}{a^2} \right) + y^2 \left(\frac{\sin^2 \theta}{b^2} + \frac{\cos^2 \theta}{a^2} \right) \right] \right\}, \quad (5)$$

with the free parameters C , a , b , and θ for, respectively, the amplitude, the semi-major and semi-minor axes (i.e., the standard deviations) of the ellipsoid, and the sub-drift angle for the orientation of the semi-major axis measured counterclockwise from the positive y -axis. More precisely, the x - (i.e., for the time lag) and y -axes (i.e., for the frequency lag) are respectively oriented horizontally and vertically on the autocorrelation plots shown in Figures 6–10 below. To find these parameters we use the `scipy.optimize.curve_fit` package, which per-

forms a non-linear least squares fit. The package also returns a covariance matrix, which is used to calculate the uncertainty of the fitted parameters. These uncertainties are then scaled by the square-root of the reduced χ^2 computed from the residual between the autocorrelation function and its Gaussian fit. We note that the uncertainty calculated this way, while useful, does not capture the entire error budget which depends more significantly on the error in the DM as well as the parts of the burst spectra that have been masked out.

Using the angle θ , the sub-burst drift rate is calculated via

$$\frac{d\nu_{\text{obs}}}{dt_D} = -\frac{\nu_{\text{res}}}{t_{\text{res}}} \cot \theta, \quad (6)$$

where ν_{res} and t_{res} are the frequency and time resolutions of the dynamic spectrum. We obtain the sub-burst duration from the fit parameters through

$$t_w = t_{\text{res}} \frac{ab}{\sqrt{b^2 \sin^2 \theta + a^2 \cos^2 \theta}}. \quad (7)$$

These expressions are also used to propagate the fit parameter uncertainties to the values of $d\nu_{\text{obs}}/dt_D$ and t_w . These are the error bars shown in Figure 1, which do not account for uncertainties in the DM or other sources.

We calculate the observation frequency ν_{obs} of each burst via an intensity-weighted average of the time-averaged frequency series. We used the `scipy.odr.RealData` package, which uses orthogonal distance regression and incorporates the uncertainties on the data to find a fit. With these measurements for ν_{obs} , as well as the drift rate $d\nu_{\text{obs}}/dt_D$ and duration t_w for each sub-burst, we plot our results for a comparison against the model described by equation (1) and in (16), as shown in Figure 1.

Since we expect a variation in the DM used to de-disperse a sub-burst to cause a rotation in its angle θ and thus a corresponding change in its measured drift rate, we varied the DM to test

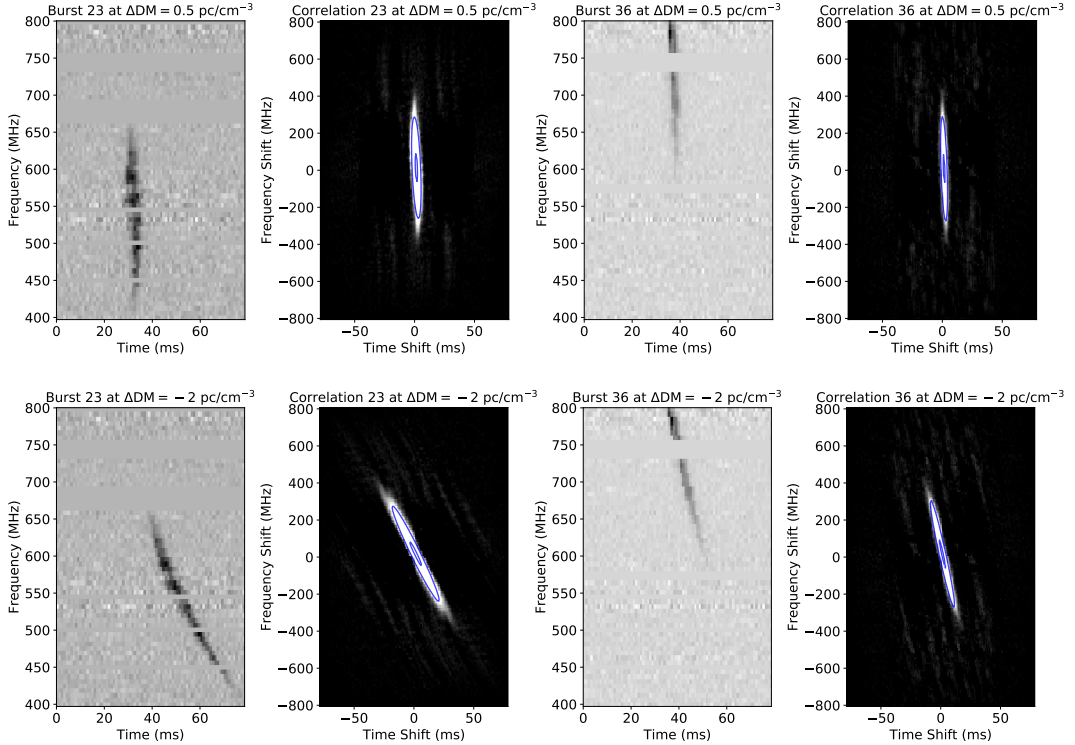


Figure 2: Changes to dynamic spectra and autocorrelation as a function of variations in the DM. Sub-bursts 23 (first column) and 36 (third column) from FRB 180916.J0158+65 are shown with their autocorrelation functions (second and fourth columns, respectively) for two offsets $\Delta\text{DM} = 0.5 \text{ pc cm}^{-3}$ (top row) and -2 pc cm^{-3} (bottom row) from the value chosen for our analysis (i.e., $\text{DM} = 348.82 \text{ pc cm}^{-3}$). The rotations brought about by the small changes in DM are clearly seen in both the dynamic spectra and autocorrelation functions.

the robustness of the relationship observed between the sub-burst drift rate and duration. That is, using the sub-bursts from FRB 180916.J0158+65 we repeated the autocorrelation analysis described above while varying the original DM of $348.82 \text{ pc cm}^{-3}$ by steps of $\Delta\text{DM} = 0.5, -1$, and -2 pc cm^{-3} , which are within the corresponding range given by (4) for this source. Values of ΔDM larger than 0.5 pc cm^{-3} yielded positive sub-burst drift rates which, according to our model, indicates over-de-dispersion (see equations (1) and (6); an increase in ΔDM will reduce the angle θ). The aforementioned rotation due to a change ΔDM can be seen in Figure 2 through the comparison of the orientation of the sub-bursts in dynamic spectra and the corresponding

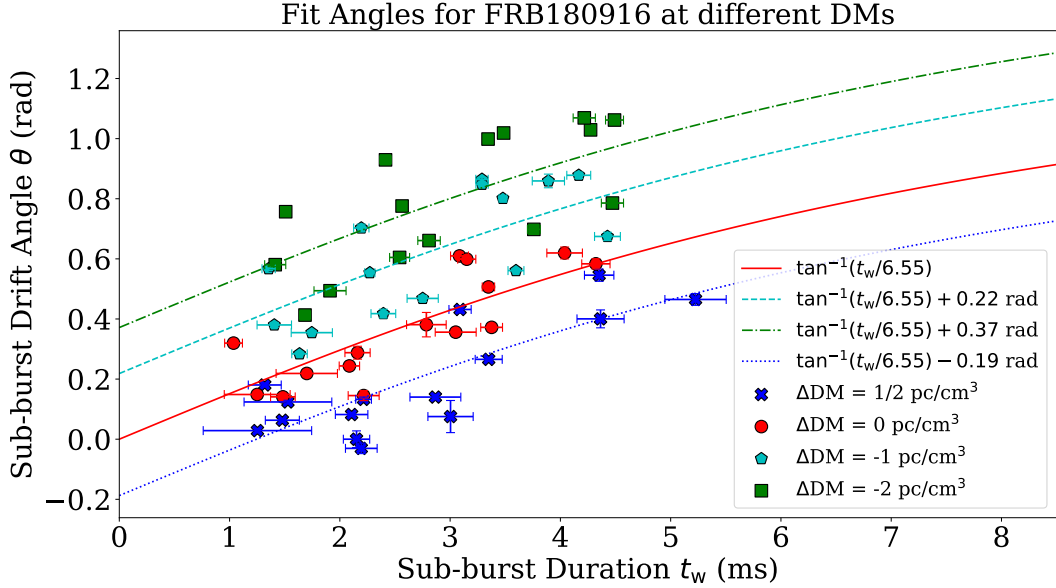


Figure 3: Robustness test: the fit angle θ vs. sub-burst duration t_w from bursts de-dispersed to small variations in the DM for the source FRB 180916.J0158+65. Red circles are sub-bursts at $\Delta\text{DM} = 0$ which corresponds to a $\text{DM} = 348.82 \text{ pc cm}^{-3}$. Blue crosses, cyan pentagons, and green squares are sub-bursts de-dispersed to $\Delta\text{DM} = 0.5, -1$, and -2 pc cm^{-3} , respectively. The red curve is fit to the red circles and is of the form given in equation (8), derived from the dynamical model described in the main text. Blue, cyan, and green curves are obtained by adding a rotation (i.e., adding an angle) to the $\Delta\text{DM} = 0$ model. This plot demonstrates the rotational effect small variations in the DM has on the autocorrelation of dynamic spectra of FRBs.

autocorrelation functions for different values for this parameter. The same effect is also clearly visible in Figure 3 for the fit angle θ and duration t_w found for the collection of sub-bursts used from FRB 180916.J0158+65 de-dispersed to the different DM values.

Using equations (1) and (6), the drift angle is related to the sub-burst duration through

$$\theta = \arctan \left(\frac{1}{A} \frac{\nu_{\text{res}}}{\nu_{\text{obs}}} \frac{t_w}{t_{\text{res}}} \right), \quad (8)$$

where as before $A \equiv \tau'_w/\tau'_D$ (see the discussion following equation (1)). We also approximated ν_{obs} to be constant, which is adequate for what follows. We find that the chosen fit obtained with equation (8) for the sub-bursts at $\Delta\text{DM} = 0$ (i.e., the red curve in Figure 3) is also satisfactory

for angles corresponding to the different ΔDM values when a simple offset is applied. We further note that the measured sub-burst duration is not strongly affected by the changes in DM. These results indicates that even though the sub-burst drift angle (and rate) is quite sensitive to the chosen DM, the relative differences between drift angles (rates) among a cohort of sub-bursts are consistent. Indeed, the expected relationship trend between the sub-burst drift rate and duration exists even for different choices of DM.

Error Introduced by Frequency Band Masking

As noted in the previous section, we first transformed our dynamic spectra via the 2D auto-correlation technique introduced in (7), and then extracted the sub-burst drift ($d\nu_{\text{obs}}/dt_{\text{D}}$) and temporal duration (t_w) via a Gaussian fit optimization procedure. In addition to random signal noise, the dynamic spectra analyzed were complicated by missing frequency bands of data, which would sometimes overlap with the frequency extent of the sub-burst under analysis. In this section we assess the error introduced by the missing frequency band data by (1) artificially masking (zero-padding) various trial Gaussian signals of known orientations and characteristic widths, (2) processing them through our pipeline, and (3) comparing the extracted sub-burst drift and duration parameters to the generating parameters.

Consider, for example, sub-burst 23 of FRB 180916.J0158+65 (18) pictured, along with its two-dimensional autocorrelation, in Figure 8. Three frequency bands of data are absent from the original data in sub-burst 23, and the total missing bandwidth (as a fraction of the frequency extent of the sub-burst) is higher than the fractional bandwidth typically absent from sub-bursts analyzed in the paper.

To estimate the effect of missing frequency channels on our analysis we construct an artificial burst from a Gaussian of $a = 90$ pixels, $b = 15$ pixels, $\theta = 10^\circ$ (inclination from vertical), and with stochastic noise of amplitude 25% that of the Gaussian amplitude. As a first test,

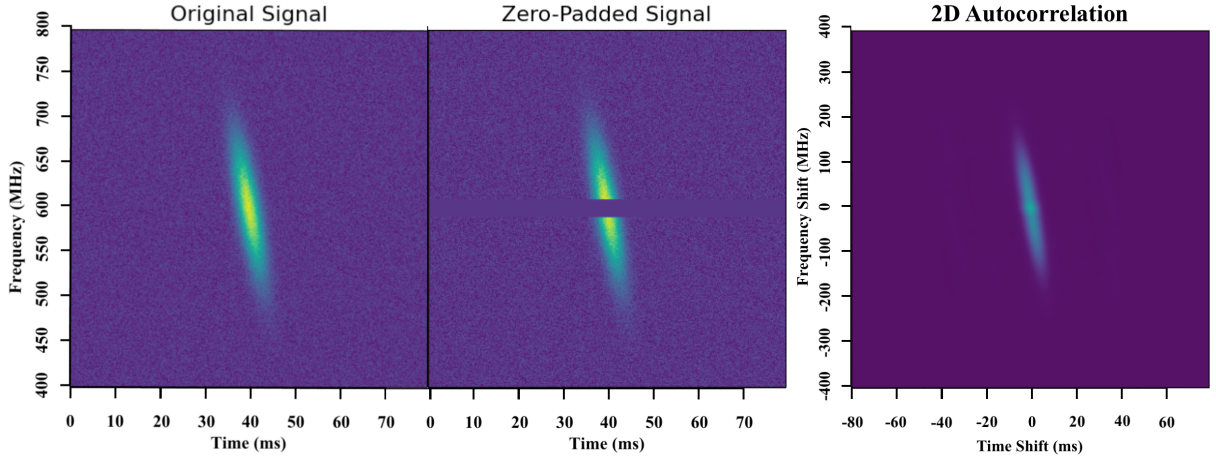


Figure 4: Artificial Gaussian signal (left), masked (zero-padded) signal (centre), and 2D autocorrelation of zero-padded signal (right). The signal shown approximately matches the characteristics of Burst 23 depicted in Figure 8 in each of their temporal widths, their frequency extents, their inclinations, and their total missing frequency bandwidths.

we mask a band of 25 pixels on the Gaussian’s vertical centre and pass this zero-padded signal through our pipeline. The fitting procedure on the 2D autocorrelation returns $a_{\text{fit}} = 102.7$ pixels, $b_{\text{fit}} = 14.8$ pixels, and $\theta_{\text{fit}} = 9.83^\circ$. The process is visualized in Figure 4. For such a small inclination angle, the percentage error in t_w is very close to that of b , and is (in this case) approximately 1%.

We can generalize this test by shifting the frequency masking band of Figure 4 vertically. We then observe that the error thus introduced is independent of the frequency band’s vertical position. The percentage error for the pulse duration is found to be $\approx (-1.4 \pm 0.4)\%$, where the $\pm 0.4\%$ uncertainty applies to all band positions tested, while the corresponding error in the angle is $\approx (-1.1 \pm 0.7)\%$.

If we now rotate the pulse of Figure 4, while retaining the central band mask of 25 pixels (where, recall for reference, $a = 90$ pixels) on pulse centre, we observe a linear enhancement of error with increasing orientation. The effect is, however, a negligible one: for every pulse rotation by 10° , the duration error increases by only 0.45%, while the orientation angle error

decreases (or increases in magnitude) by only 0.12° .

The narrow-band nature of the emission process

Following the model of Rajabi et al. (2020) (16), the temporal duration of an FRB sub-burst in the observer rest frame is given by

$$t_w = \tau'_w \frac{\nu_0}{\nu_{\text{obs}}}, \quad (9)$$

where, as defined in the main text, τ'_w , ν_0 and ν_{obs} respectively are the proper temporal width and frequency of emission in the FRB rest frame, as well as the frequency of the signal as measured by the observer. Equation (9) clearly predicts an inverse relationship between the observed FRB temporal width and frequency, which had previously been noticed and studied. For example, a verification of this effect can be found in Figure 7(b) of (6) for the case of FRB 121102. Although the burst temporal duration exhibits a fair amount of scattering at a given frequency (inherent to τ'_w in equation (9)), the predicted behavior is clearly observed. Since the data used for this source come from observations spanning a wide range of frequencies, it further follows from equation (9) that the rest frame frequency ν_0 cannot change significantly as a function of ν_{obs} , as this would affect the inverse relationship observed in the data.

Rajabi et al. (2020) (16) also derived the following equation for the drift in the observed central frequency of a sequence of sub-bursts with increasing arrival time

$$\frac{\Delta\nu_{\text{obs}}}{\Delta t_D} = \frac{\nu_{\text{obs}}}{\nu_0} \frac{d\nu_{\text{obs}}}{d\tau'_D}, \quad (10)$$

where the term on the left-hand side is for the central frequency drift and τ'_D is the proper temporal delay between the arrival of the trigger and the emission of the ensuing sub-burst in the FRB rest frame. The derivative $d\nu_{\text{obs}}/d\tau'_D$ is a physical parameter characterizing the environment of the FRB source, which determines whether the sequence of sub-bursts has the appearance of a “sad” ($d\nu_{\text{obs}}/d\tau'_D < 0$) or “happy trombone” ($d\nu_{\text{obs}}/d\tau'_D > 0$; see (16) for more

details). Equation (10) predicts that the central frequency drift should scale linearly with ν_{obs} , which has previously been verified for FRB 121102 over a wide range of frequencies. This can be asserted, for example, from Figure 3 (top panels) of Hessels et al. (2019) (7). Once again, this observed dependency could not be realized if ν_0 changed significantly in equation (10).

Finally, equation (9) can be inserted in equation (1) to obtain

$$\frac{1}{\nu_{\text{obs}}^2} \frac{d\nu_{\text{obs}}}{dt_D} = -\frac{1}{\nu_0 \tau'_D}, \quad (11)$$

for the sub-burst drift (normalized to ν_{obs}^2), which is then predicted to be independent of ν_{obs} and scale inversely with ν_0 . Figure 5 shows the corresponding plot using the same data as in Figure 1. The broken black line is for a fit to a constant B on the combined data for the three sources, with $B \equiv (\tau'_D \nu_0)^{-1} = (2.1 \pm 0.2) \times 10^{-8}$. While there is some scatter in the data, the expected lack of dependency with ν_{obs} is observed, any deviation can easily be accounted for with the uncertainty on the DMs. As was the case for the temporal narrowing and sad trombone effect discussed above for FRB 121102, this behavior would be affected if ν_0 changed significantly in equation (11).

Taken together the verification of these three predictions provide strong evidence that the underlying physical process responsible for the emission of FRB signals in these repeating FRBs is narrow-band in nature.

Determination of β^+ , ν_0 and $\Delta\beta'$

The equations presented in this section apply to cases where the source of radiation travels directly toward or away from the observer.

For the determination of the maximum speed of an FRB rest frame toward the observer $\beta^+ > 0$ and ν_0 , the frequency of emission within it, we can generally set $\beta^- = -a\beta^+$ with

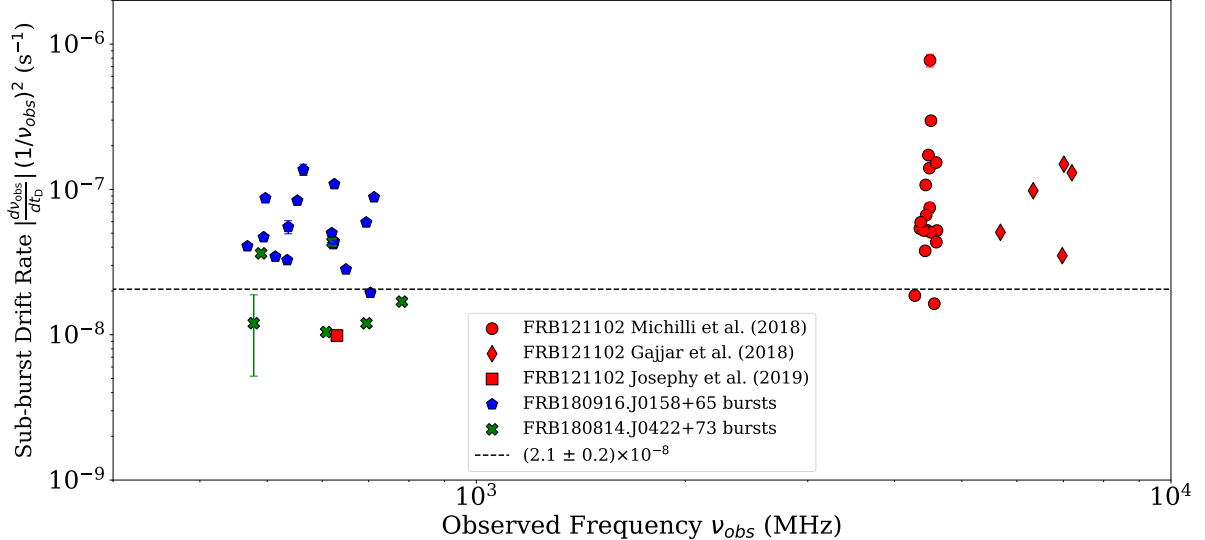


Figure 5: A plot of $(1/\nu_{\text{obs}}^2) |d\nu_{\text{obs}}/dt_D|$ vs. ν_{obs} for FRB 121102 (red circles, diamonds and square) (6, 9, 27), FRB 180916.J0158+65 (blue pentagons) (18) and FRB 180814.J0422+73 (green crosses) (8). The broken black line is for a fit to a constant B on the combined data for the three sources, with $B \equiv (\tau'_D \nu_0)^{-1} = (2.1 \pm 0.2) \times 10^{-8}$. Error bars shown only account for uncertainties derived from the underlying Gaussian fit of the autocorrelation function and do not reflect uncertainties caused by, for example, de-dispersion of the data.

$a \geq 0$ for the greatest (i.e., most negative) speed away from the observer. Using the relativistic Doppler shift formula (35) for the corresponding frequencies in the observer's rest frame

$$\nu_{\text{obs}}^{\pm} = \nu_0 \sqrt{\frac{1 + \beta^{\pm}}{1 - \beta^{\pm}}}, \quad (12)$$

we find that

$$\beta^+ = \left(\frac{1+a}{2a} \right) \left(\frac{\nu_{\text{obs}}^+{}^2 + \nu_{\text{obs}}^-{}^2}{\nu_{\text{obs}}^+{}^2 - \nu_{\text{obs}}^-{}^2} \right) \left[1 - \sqrt{1 - \frac{4a}{(1+a)^2} \left(\frac{\nu_{\text{obs}}^+{}^2 - \nu_{\text{obs}}^-{}^2}{\nu_{\text{obs}}^+{}^2 + \nu_{\text{obs}}^-{}^2} \right)^2} \right] \quad (13)$$

$$\nu_0^2 = \nu_{\text{obs}}^+ \nu_{\text{obs}}^- \sqrt{\frac{1 - (1-a)\beta^+ - a\beta^{+2}}{1 + (1-a)\beta^+ - a\beta^{+2}}}. \quad (14)$$

The discussion in the main text where the FRB rest frames span the range $\pm\beta^+$ corresponds to the case $a = 1$, which reduces equations (13)-(14) to equations (2)-(3). We also note that a

system becomes most strongly relativistic when $a \rightarrow 0$ where $\nu_0 \rightarrow \nu_{\text{obs}}^-$, while the opposite is true as $a \rightarrow \infty$ and $\nu_0 \rightarrow \nu_{\text{obs}}^+$.

For the determination of $\Delta\beta'$, we start by considering that for a signal initially observed at frequency ν_{obs} a velocity change $\Delta\beta$ in the observer's rest frame will be accompanied by a change $\delta\nu_{\text{obs}}$ in frequency given by

$$\frac{\delta\nu_{\text{obs}}}{\nu_{\text{obs}}} = \frac{\Delta\beta}{1 - \beta^2}, \quad (15)$$

where β is the initial velocity relative to the observer. Using the special relativistic velocity addition law (35) we can relate the velocity changes in the observer and FRB rest frames through

$$\Delta\beta = \Delta\beta' \left(\frac{1 - \beta^2}{1 + \beta\Delta\beta'} \right), \quad (16)$$

with $\Delta\beta'$ the corresponding velocity change in the FRB frame.

Allowing for the motions within the FRB rest frame to span the range $\pm\Delta\beta'$ (with $\Delta\beta' \geq 0$; for simplicity, we assume a symmetric velocity range about zero), while using equations (12) (to express β as a function of ν_{obs} and ν_0) and (15)-(16), we find the following relation for the total observed bandwidth covered by the corresponding signals

$$\frac{\Delta\nu_{\text{obs}}}{\nu_{\text{obs}}} = 2\Delta\beta' \left[1 - \Delta\beta'^2 \left(\frac{\nu_{\text{obs}}^2 - \nu_0^2}{\nu_{\text{obs}}^2 + \nu_0^2} \right)^2 \right]^{-1}. \quad (17)$$

Equation (4) of the main text follows from this relation, which reaches a maximum value when $\nu_{\text{obs}} = 0$ or $\nu_{\text{obs}} \gg \nu_0$. While equation (17) shows little variations whenever $\Delta\beta' \ll 1$, it could, in principle, be used to evaluate the FRB rest frame frequency ν_0 independently of equation (14) since it reaches a minimum of $2\Delta\beta'$ at $\nu_{\text{obs}} = \nu_0$. However, the effect is probably too small (on the order of 1% for FRB 121102) to be measurable given the scatter inherent to FRB data.

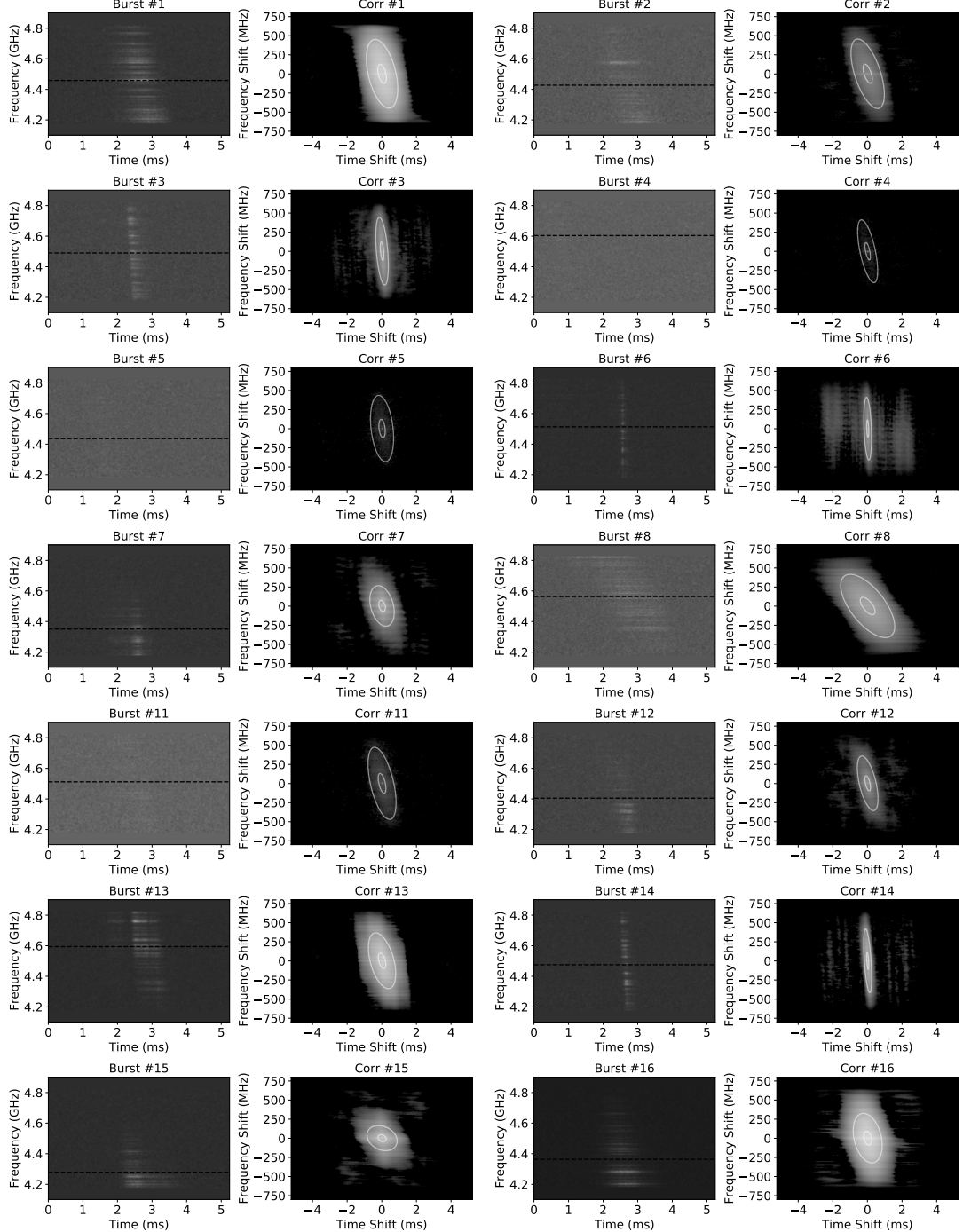


Figure 6: Dynamic spectra (first and third columns) and corresponding autocorrelation functions (second and fourth columns) for FRB 121102 bursts at a frequency of approximately 4–5 GHz from (27). The dynamic spectra were de-dispersed with a DM = 559.7 pc cm⁻³ and the dashed horizontal line in the dynamic spectra denotes the center frequency ν_{obs} used for the analysis. The autocorrelation functions are modelled with a 2D Gaussian ellipsoid whose one- and two-standard deviation levels are shown using the white contours.

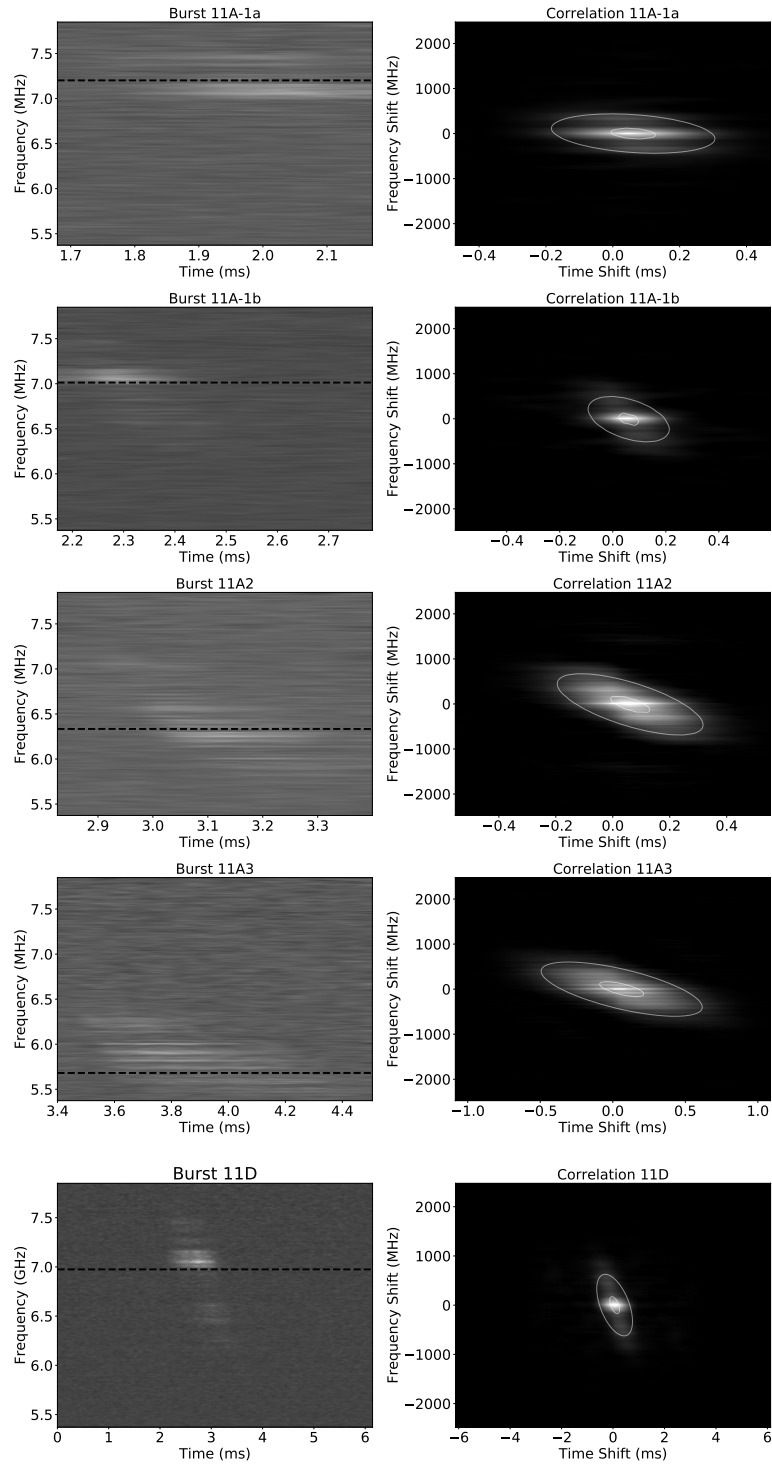


Figure 7: Same as Figure 6 but for the FRB 121102 data at approximately 5–8 GHz published in (6) and de-dispersed with a $\text{DM} = 565 \text{ pc cm}^{-3}$. The top four sub-bursts are taken from one event, i.e., Burst 11A. Note that the time axes for the autocorrelation functions do not all share the same range, which distorts their relative appearance.

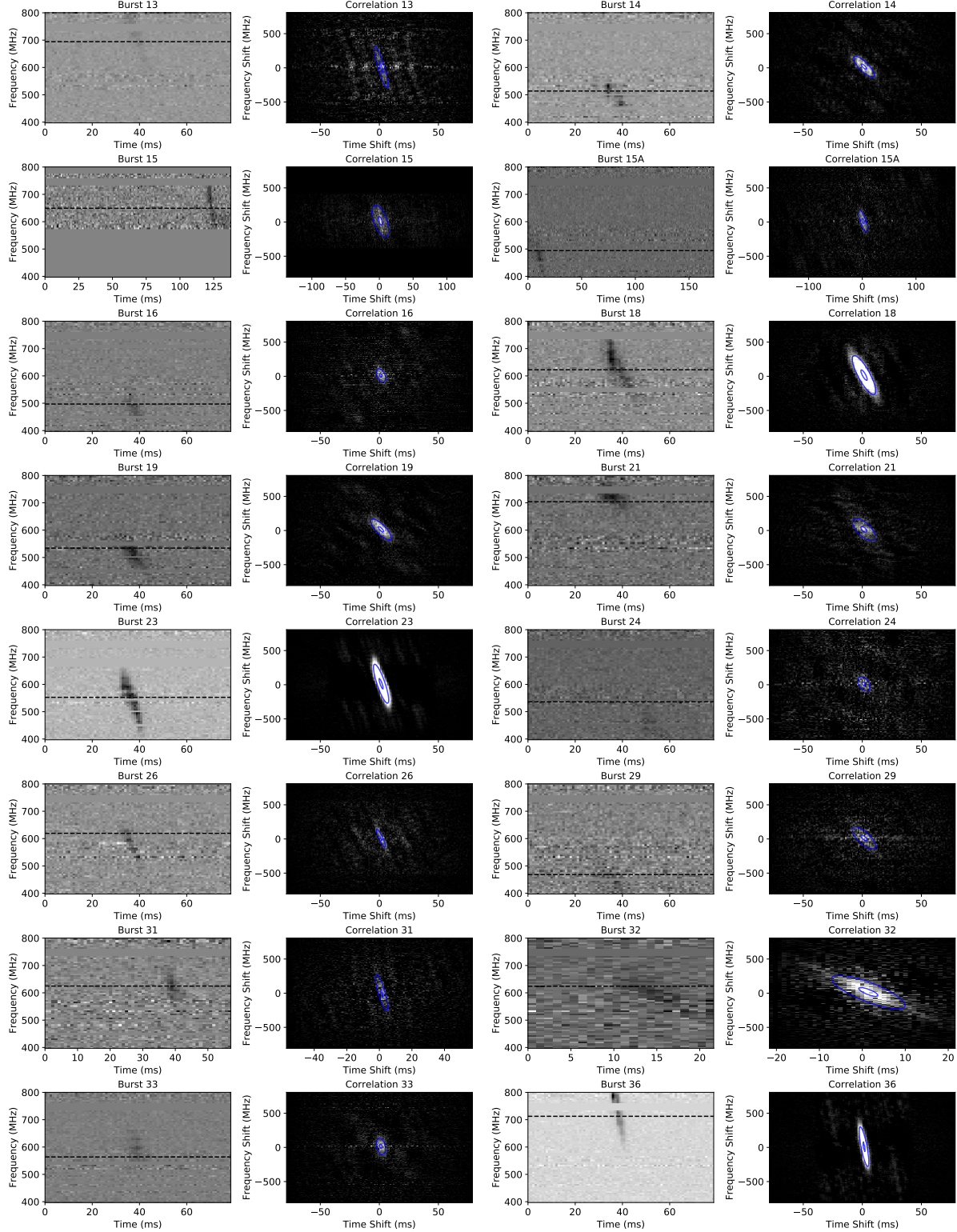


Figure 8: Same as Figure 6 but for FRB 180916.J0158+65 taken from (18). These data were de-dispersed with a $\text{DM} = 348.82 \text{ pc cm}^{-3}$. Note that the time axes for the autocorrelation functions do not all share the same range, which distorts their relative appearance.

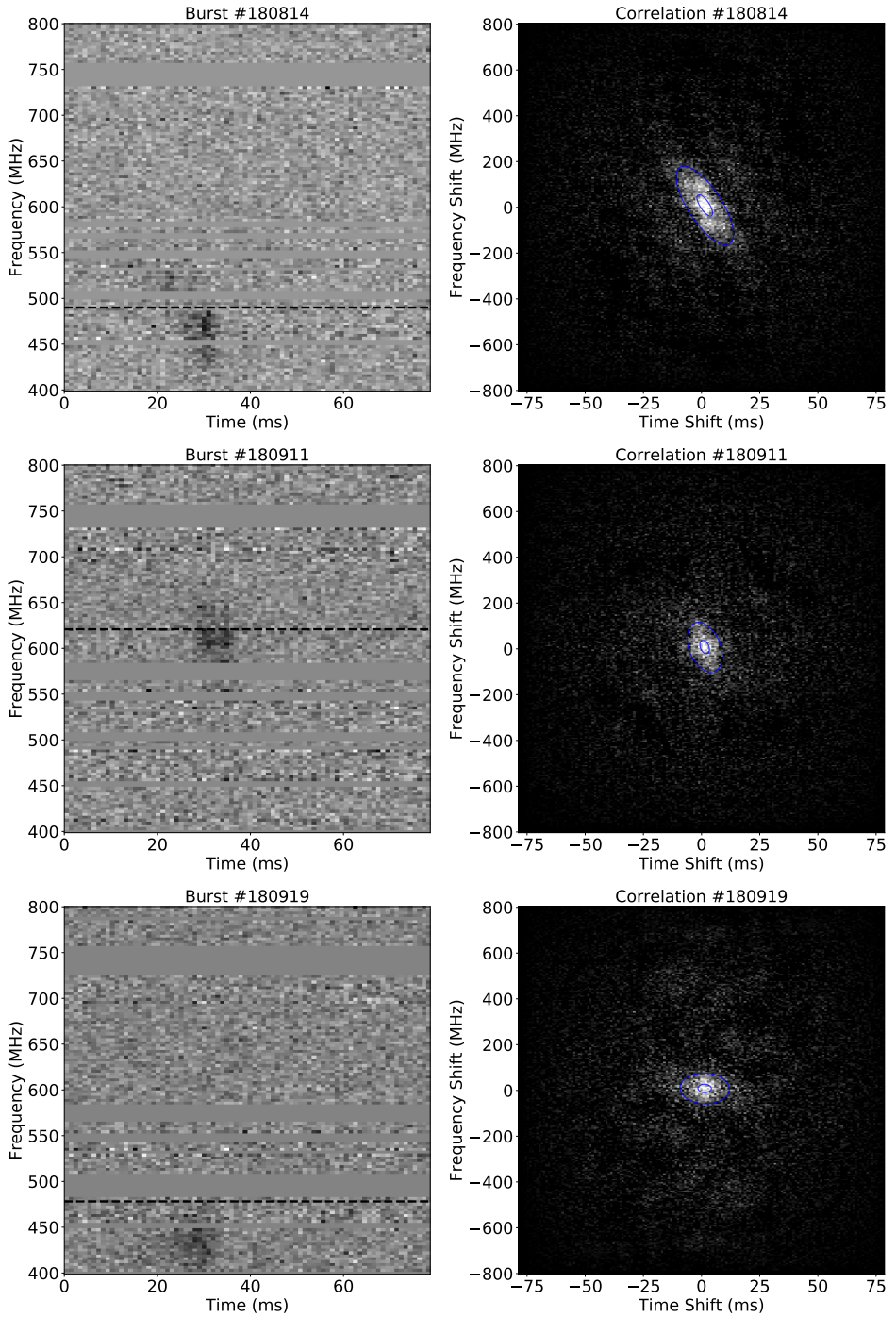


Figure 9: Same as Figure 6 but for FRB 180814.J0422+73 taken from (8). These data were de-dispersed with a $\text{DM} = 188.9 \text{ pc cm}^{-3}$.

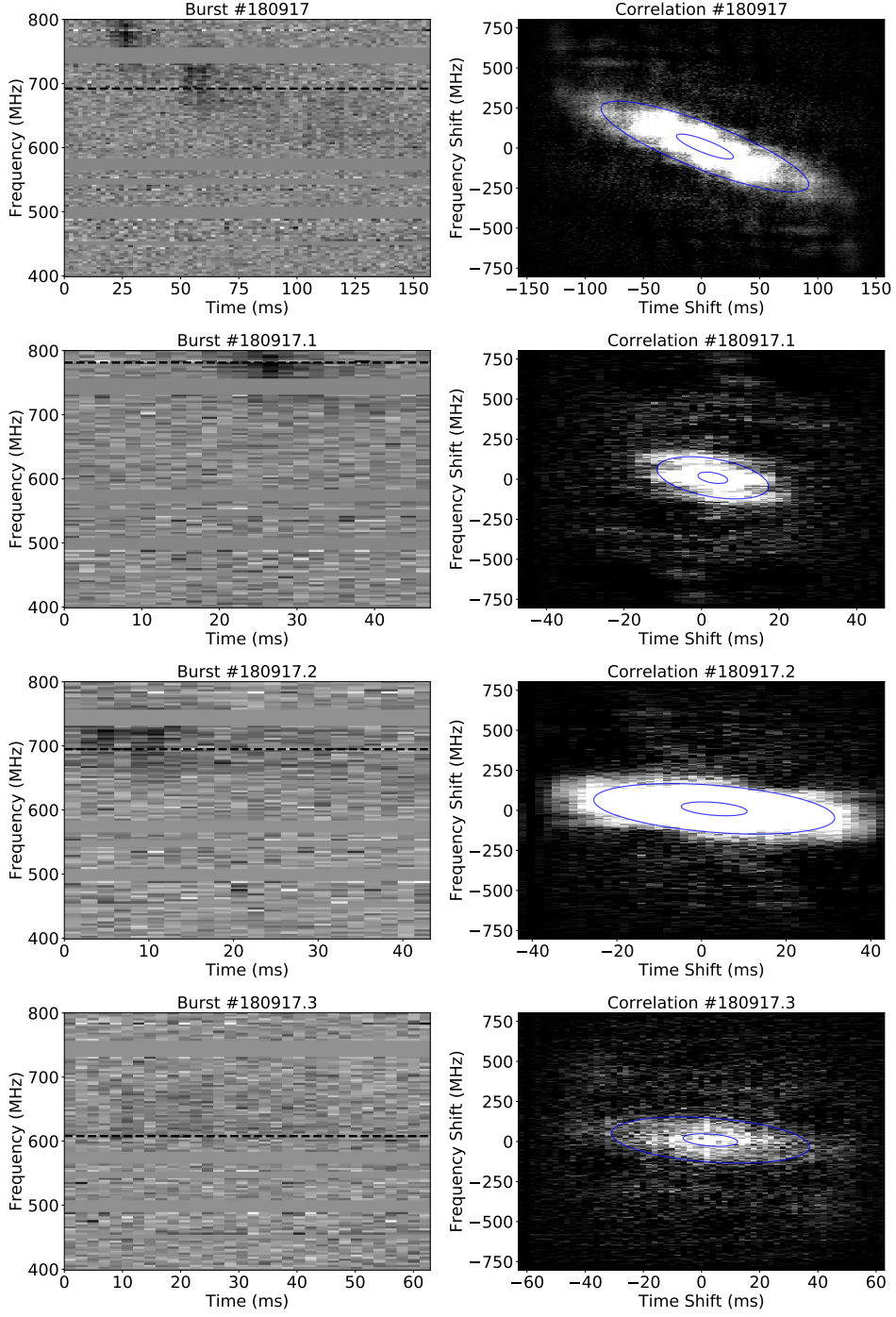


Figure 10: Same as Figure 9 but for Burst #180917 of FRB 180814.J0422+73 taken from (8). The whole event is shown on the top row (not used for Figure 1), while its three separate sub-bursts are detailed in the bottom three (all used for Figure 1). Note that the time axes for the autocorrelation functions do not all share the same range, which distorts their relative appearance.